RSC Advances

PAPER

View Article Online
View Journal | View Issue

Check for updates

Cite this: *RSC Adv.*, 2019, **9**, 28207

Ultra-small dispersed Cu_xO nanoparticles on graphene fibers for miniaturized electrochemical sensor applications†

Jinfeng Zeng,[a] Xiaoteng Ding,[b] Liwei Chen,[a] Le Jiao,[a] Yuze Wang,[a] Christopher D. Windle,[c] Qing Han *[a] and Liangti Qu [a]

Received 20th May 2019
Accepted 28th August 2019

DOI: 10.1039/c9ra03802g

rsc.li/rsc-advances

A graphene microfiber (GF) modified with ultrafine Cu_xO nanoparticles (Cu_xONPs/GF) has been fabricated by direct annealing of electrodeposited nano-sized copper-based metal organic frameworks (HKUST-1) and used as an electrode for nonenzymatic H_2O_2 sensing. Benefiting from the unique microfiber architecture and synergetic effects, as well as strong coupling between components with many active sites and boosted electron transport, the Cu_xONPs/GF electrode shows prominent sensitivity, selectivity and long-term operational stability for the detection of H_2O_2. Further work successfully applied this Cu_xONPs/GF electrode to detection of H_2O_2 in real samples such as milk and human serum. These results indicate that the Cu_xONPs/GF is a promising mini-sized sensor in electrochemical analysis.

Open Access Article. Published on 09 September 2019. Downloaded on 1/22/2026 3:10:54 AM.
This article is licensed under a Creative Commons Attribution-NonCommercial 3.0 Unported Licence.

Introduction

The demand for electrochemical sensors with high sensitivity, low cost, excellent selectivity, and facile miniaturization has stimulated extensive research into developing versatile materials with remarkable electrocatalytic activity. Compared to conventional macro-electrodes,[1] fiber-type electrodes with a one-dimensional microstructure, particularly carbon fiber microelectrodes possessing one dimensional diffusion, have been widely fabricated and used in sensors due to their low cost, small volume, portability and good biocompatibility. However, the poor electrocatalytic activity and low current response of carbon fiber microelectrodes seriously restrict their application in sensing.

Graphene has potential as an electrode for electrochemical analysis owing to its large specific surface area, excellent electron mobility, high mechanical properties and good biocompatibility. Recently, we reported a graphene fiber assembled with chemically reduced graphene sheets, which exhibited promising electrochemical sensing activity, mainly owing to the inherent defects and residual oxygenated functional groups as active sites. However, the weak electrocatalytic properties of graphene restrict its wide application in electrochemical analysis. It is revealed that combining graphene fiber with catalytically active nanomaterials such as metals and metal oxides is an efficient way to enhance the electrocatalytic activity.[2–12] Copper oxide nanoparticles (Cu_xONPs) are an attractive alternative electroactive species due to their abundance, low cost, good chemical stability and unique electronic properties.[13,14] Hybridizing graphene with Cu_xONPs is an effective way, where the composite materials have fully exploited the structural merits of individual components and improved the analytic performance. So far, various strategies, including thermal conversion,[15] ion exchange,[16] wet chemistry,[17] microwave,[18] template growth,[19] and anion-assisted approaches[20] have been employed to prepare Cu_xONPs/graphene hybrids. Unfortunately, as-prepared Cu_xONPs from these approaches suffer from aggregation on graphene-based materials, leading to poor dispersion and a low number of active sites with poor electrocatalytic performance. In addition, although Cu_xONPs/graphene composites have been widely investigated and demonstrated with great potential for electrochemical analysis, there is still a lack of exploration for its miniaturized sensors. Thus, it is urgent to design and develop a simple and effective method for the production of Cu_xONPs/graphene fiber-based microsensor with a high number of active sites and highly efficient electrocatalytic activity.

Hydrogen peroxide (H_2O_2) is indispensable to ecosystems and is widely used in foodstuffs, the environment, medicine and industry. Excess H_2O_2 can lead to toxicity for humans and to the environment.[21–24] Although electrochemical enzyme-based sensors have good selectivity and high performance, their applications are limited because of their poor stability and high cost. Therefore, the development of non-enzymatic sensors has drawn tremendous attention. Herein, we report

[a]Key Laboratory of Photoelectronic/Electrophotonic Conversion Materials, Key Laboratory of Cluster Science, Ministry of Education of China, School of Chemistry and Chemical Engineering, Beijing Institute of Technology, Beijing 100081, P. R. China. E-mail: qhan@bit.edu.cn

[b]College of Life Sciences, Qingdao University, Qingdao 266071, P. R. China

[c]Solar Energy and Advanced Materials Group, Department of Chemical Engineering, University College London, Torrington Place, London, WC1E 7JE, UK

† Electronic supplementary information (ESI) available: Additional Fig. S1–S7, Tables S1 and S2, and more discussions. See DOI: 10.1039/c9ra03802g

Open Access Article. Published on 09 September 2019. Downloaded on 1/22/2026 3:10:54 AM.
This article is licensed under a Creative Commons Attribution-NonCommercial 3.0 Unported Licence.

a graphene microfiber electrode modified by well-dispersed and ultrafine Cu_xO nanoparticles (Cu_xONPs/GF) derived from copper-based metal organic frameworks (HKUST-1) by a direct electrodeposition self-assembly technique for nonenzymatic electrochemical H_2O_2 detection. The unique nanoarchitecture and synergetic effect as well as strong coupling between components endows them with a high density of active sites and enhanced electron transport leading to improved electrochemical micro-sensing. The resulting hybrid fiber electrode exhibits a very low detection limit of 0.023 μM and a rapid response time of 1 s. Our work provides a straightforward method for synthesizing highly efficient nonenzymatic microsensing electrodes for H_2O_2 detection.

Experimental

Synthesis of graphene fiber (GF)

Graphene oxide (GO) was synthesized by oxidation of graphite powder according to the modified Hummers' method.[25] Then, graphene oxide fibers (GOF) were prepared by a wet spinning strategy. Typically, 3 mL GO (20 mg mL^{-1}) was spun into a methanol solution saturated by potassium chloride (KCl) with a speed of 0.1 m s^{-1} by an injector (with a diameter of 0.25 mm), followed by drying. To obtain GF, the GOF was heated to 200 °C for 2 h at first and then further heated to 1000 °C for 2 h with a heating rate of 10 °C min^{-1} under N_2/H_2 (v/v = 4 : 1) atmosphere.

Synthesis of HKUST-1 nanoparticles decorated GF (HNPs/GF)

A two-electrode system was used for the preparation of HNPs/GF (HNPs = HKUST-1 nanoparticles). Firstly, 0.2416 g of cupric nitrate trihydrate ($Cu(NO_3)_2 \cdot 3H_2O$), 0.2102 g of 1,3,5-benzenetricarboxylic acid (H_3BTC) and 0.7748 g of tetrabutylammonium hexafluorophosphate (NBu_4PF_6) were dispersed in 20 mL of *N*,*N*-dimethylformamide (DMF) solution, and the mixture was treated by ultrasound for 30 min to obtain a homogeneous solution. Next, the as-synthesized GF (2.0 mm length) and a commercial Pt plate were used as the working electrode and counter electrode, respectively. The HNPs/GF was fabricated by the electrodeposition of HNPs on the GF surface in the above mixed solution (degassed with N_2 for 30 min) at −1.5 V for 60 s, the obtained sample is denoted $HNPs_{60}$/GF. For comparison, a series of HNPs/GF samples with different amounts of HNPs were obtained by adjusting the electrodeposition time (30 s, 90 s, and 120 s) in the same mixed solution, which were denoted $HNPs_{30}$/GF, $HNPs_{90}$/GF and $HNPs_{120}$/GF, respectively.

Synthesis of Cu_xONPs/GF

The Cu_xONPs/GF was synthesized by direct annealing of HNPs/GF ($HNPs_{30}$/GF, $HNPs_{60}$/GF, $HNPs_{90}$/GF and $HNPs_{120}$/GF) samples from room temperature to 400 °C in N_2 with a ramp rate of 10 °C min^{-1} and stabilized for 2 h, then cooled to room temperature naturally, and denoted $Cu_x ONPs_{30}/GF_{400}$, $Cu_x ONPs_{60}/GF_{400}$, $Cu_x ONPs_{90}/GF_{400}$ and $Cu_x ONPs_{120}/GF_{400}$, respectively.

In order to study the influence of the annealing temperature on the performance of the final samples, a series of Cu_xONPs/GF samples were obtained by annealing the $HNPs_{60}$/GF sample at 300 °C and 500 °C, respectively. The obtained samples were denoted $Cu_x ONPs_{60}/GF_{300}$ and $Cu_x ONPs_{60}/GF_{500}$, respectively.

Synthesis of Cu_xONPs/GF electrode

The Cu_xONPs/GF was glued with silver conductive adhesive onto stainless steel sheets (2.5 × 0.5 cm). The end of the tip was sealed with molten paraffin. The exposed Cu_xONPs/GF was cut down to 2.0 mm in length and used as the electrode. The exposed stainless steel sheet was then connected with the electrochemical workstation.

Results and discussion

The procedure for the fabricated Cu_xONPs/GF is shown in Fig. 1. Firstly, GO suspension (Fig. 1a) was converted into a GO fiber (GOF, Fig. 1b) by a wet spinning strategy. After drying naturally, the GOF was thermally reduced to graphene fiber (GF, Fig. 1c). The obtained GF with a diameter of 44 μm appears as wrinkled sheet-like surface morphologies (Fig. S1†). Then, electrodeposition self-assembly of the copper MOF (HKUST-1 nanoparticles, HNPs) occurred in a mixed solution containing cupric nitrate trihydrate ($Cu(NO_3)_2 \cdot 3H_2O$) and 1,3,5-benzenetricarboxylic acid (H_3BTC), in which HNPs grew *in situ* on the surface of GF after 60 s of electrodeposition ($HNPs_{60}$/GF, Fig. 1d), which was confirmed by X-ray diffraction (XRD, Fig. S2†). As shown in Fig. 2a, the obtained $HNPs_{60}$/GF shows fiber features with a diameter of 45 μm, larger than that of the bare GF. Fig. 2b demonstrates that the $HNPs_{60}$ with an octahedral structure have a uniform size of 200 nm and are well distributed over the surface of GF. Further annealing at 400 °C led to pyrolysis of $HNPs_{60}$ with simultaneous formation of Cu_xO

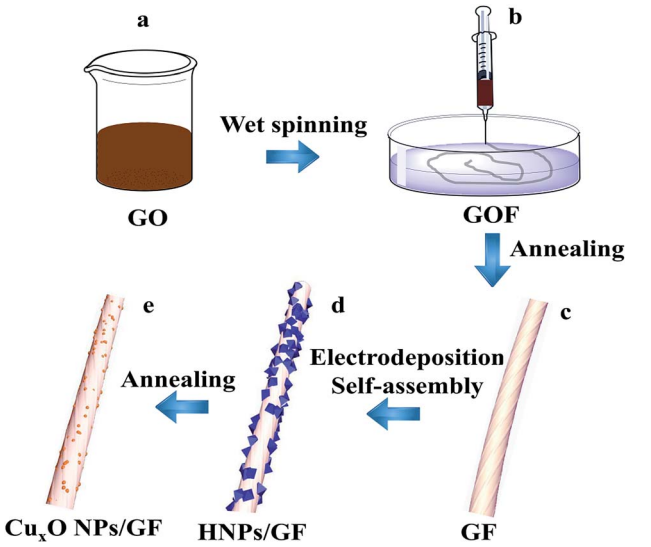

Fig. 1 Schematic illustration of the preparation of Cu_xONPs/GF. (a) GO solution, (b) GOF, (c) GF, (d) HNPs/GF, (e) Cu_xONPs/G.

This journal is © The Royal Society of Chemistry 2019

Open Access Article. Published on 09 September 2019. Downloaded on 1/22/2026 3:10:54 AM.
This article is licensed under a Creative Commons Attribution-NonCommercial 3.0 Unported Licence.

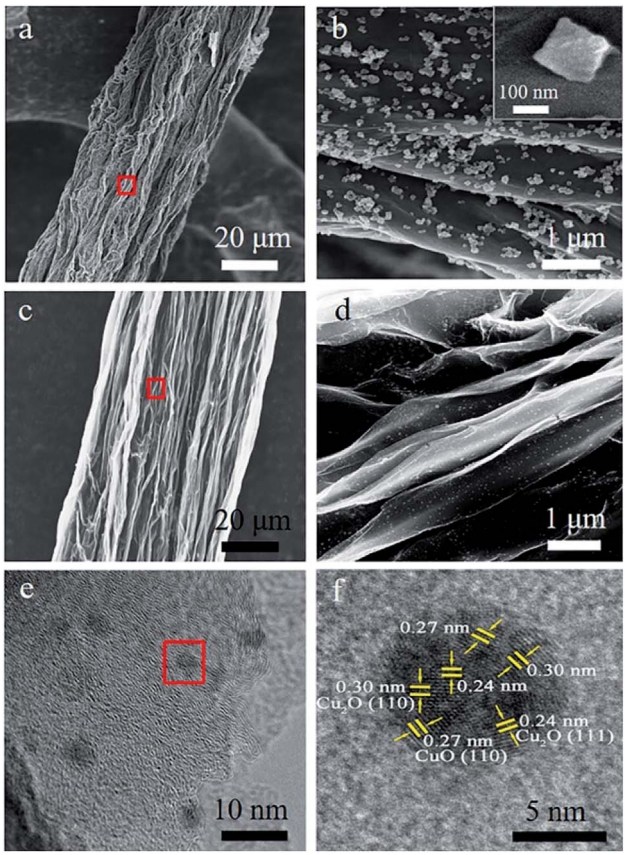

Fig. 2 (a) Scanning electron microscopy (SEM) images of $HNPs_{60}$/GF. (b) The enlarged view of the rectangle area in (a). The inset in (b) is an enlarged SEM image of a single $HNPs_{60}$. (c) SEM image of Cu_xONPs_{60}/GF_{400}. (d) The enlarged view of the rectangle area in (c). (e) Transmission electron microscopy (TEM) image of sheets within the Cu_xONPs_{60}/GF_{400}. (f) The enlarged view of the rectangle area in (e).

nanoparticles (Cu_xONPs_{60}, the size is about 10 nm) well distributed on the sheets of GF (Cu_xONPs_{60}/GF_{400}, Fig. 2c–e). High-resolution transmission electron microscopy (HR-TEM) of Cu_xONPs/GF (Fig. 2f) indicates clear lattice fringes with a spacing of 0.24, 0.27 and 0.30 nm, corresponding to the $Cu_2O(111)$, $CuO(110)$ and $Cu_2O(110)$, respectively.[26–30] Element mapping reveals the coexistent and uniform distribution of C, O and Cu elements for Cu_xONPs_{60}/GF_{400} (Fig. 3a). An X-ray photoelectron spectrum (XPS) of the bare GF shows C 1s (284.6 eV) and O 1s (531.2 eV) peaks. Apart from the C 1s and O 1s peaks observed in the GF, the Cu_xONPs_{60}/GF_{400} shows the two apparent Cu $2p_{3/2}$ and Cu $2p_{1/2}$ features at 934.2 eV and 944.4 eV with a Cu atomic percentage of 0.76% (Fig. 3b), indicating the presence of Cu_xONPs_{60}, which is consistent with the energy-dispersive X-ray spectroscopy measurement (EDS, Fig. S3 and Table S1†). The ratio of C/O decreases from 11.1 (GF) to 8.4 (Cu_xONPs_{60}/GF_{400}), demonstrating an increase in the oxygen content resulting from the introduction of Cu_xO. In addition, the chemical states of copper in Cu_xONPs_{60}/GF_{400} are revealed by the high-resolution XPS spectra (Fig. 3c). The signals of Cu $2p_{3/2}$ and Cu $2p_{1/2}$ can each be deconvoluted into two peaks of Cu_2O (933.4 eV and 935.4 eV) and CuO (941.9 eV and 944.2 eV)[31] ascribed to the oxidation products of HNPs after annealing.

H_2O_2-sensing properties

The electrochemical properties of the Cu_xONPs_{60}/GF_{400} electrode are investigated in 0.1 M PBS saturated with N_2 at a scan rate of 50 mV s^{-1}. Considering the electrodeposition self-assembly time has a significant effect on the content and size of Cu_xONPs, as well as the catalytic performance of the Cu_x-ONPs/GF electrode, various Cu_xONPs/GF electrodes were obtained by adjusting the electrodeposition self-assembly time (30 s, 90 s and 120 s), which were denoted Cu_xONPs_{30}/GF_{400}, Cu_xONPs_{90}/GF_{400}, and Cu_xONPs_{120}/GF_{400}, respectively. The SEM images and EDS analysis of the Cu_xONPs/GF samples (Fig. S4 and Table S1†) imply that with the increasing time of electrodeposition self-assembly, the content and size of the Cu_xONPs increase. As a result, there is almost no reductive peak at the Cu_xONPs_{30}/GF_{400} electrode (Fig. 4a), which can be attributed to only trace amounts of Cu_xO with inferior electrocatalytic activity (Fig. S4a and b and Table S1†). In comparison, an obviously reductive peak (about −0.05 V) was observed for the Cu_xONPs_{60}/GF_{400} electrode, which was attributed to the successful electrode surface reaction process.

A further increase of electrodeposition self-assembly time causes severe agglomeration of Cu_xONPs with a reduction in the number of active sites (Fig. S4e–h†) resulting in a decrease in the current response. The annealing temperature also has a significant effect on the size of Cu_xONPs and performance of

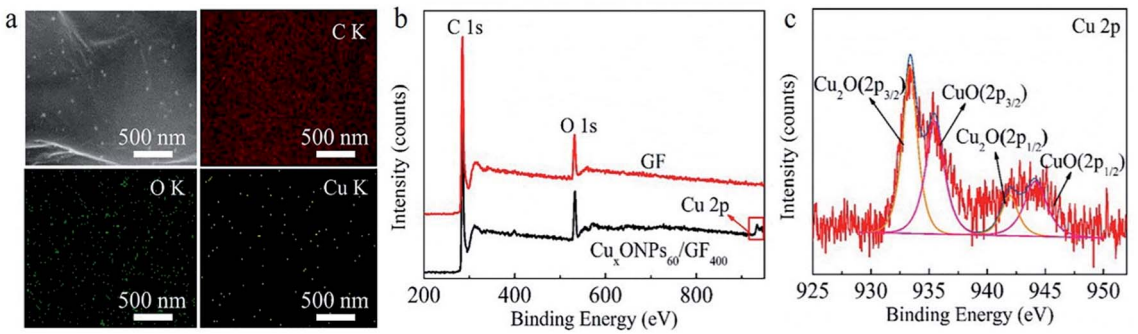

Fig. 3 (a) Scanning transmission electron microscopy (STEM) and C-, O- and Cu-element mappings for the sheets within the Cu_xONPs_{60}/GF_{400}. (b) XPS spectra of the Cu_xONPs_{60}/GF_{400} and the bare GF. (c) High-resolution Cu 2p XPS spectrum of Cu_xONPs_{60}/GF_{400}.

Open Access Article. Published on 09 September 2019. Downloaded on 1/22/2026 3:10:54 AM.
This article is licensed under a Creative Commons Attribution-NonCommercial 3.0 Unported Licence.

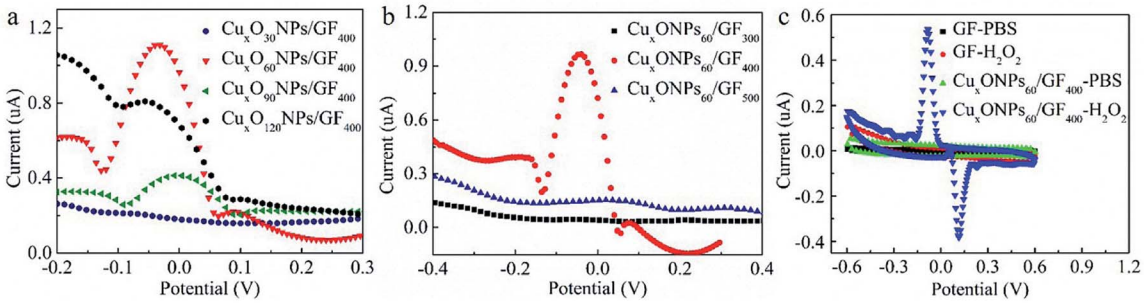

Fig. 4 (a) Differential pulse voltammograms (DPVs) of the Cu_xONPs_{30}/GF_{400}, Cu_xONPs_{60}/GF_{400}, Cu_xONPs_{90}/GF_{400} and Cu_xONPs_{120}/GF_{400} in 0.1 M phosphate buffer solution (PBS) with 0.2 mM H_2O_2 (pH = 7.15). (b) DPVs of the Cu_xONPs_{60}/GF_{300}, Cu_xONPs_{60}/GF_{400} and Cu_xONPs_{60}/GF_{500} in 0.1 M PBS with 0.2 mM H_2O_2 (pH = 7.15). (c) Cyclic voltammograms (CVs) of the bare GF and the Cu_xONPs_{60}/GF_{400} electrodes in 0.1 mM PBS (pH = 7.15) without and with 0.2 mM H_2O_2.

the final Cu_xONPs/GF electrode. For comparison, a series of Cu_xONPs/GF electrodes were prepared by annealing the precursors of HNPs/GF derived from the optimal electrodeposition time at different temperatures (300 °C and 500 °C, which were denoted Cu_xONPs_{60}/GF_{300} and Cu_xONPs_{60}/GF_{500}, respectively). Apparently, the current response signal of the Cu_xONPs_{60}/GF_{400} electrode is obviously higher than that of the Cu_xONPs_{60}/GF_{300} and the Cu_xONPs_{60}/GF_{500} electrodes (Fig. 4b). This may be attributed to the incomplete decomposition of the $HNPs_{60}$ precursor for the Cu_xONPs_{60}/GF_{300} electrode (Fig. S5a†). The residual non-conductive $HNPs_{60}$ inhibit electron transport on the surface of GF, leading to poor electrocatalytic activity towards H_2O_2 sensing. For the Cu_xONPs_{60}/GF_{500} electrode, an increase of Cu_xONPs_{60} size can be observed as shown in Fig. S5b,† hence reducing the utilization of active sites and leading to a decrease in electrocatalytic performance.[32]

As a result, compared with the bare GF (no redox peaks, Fig. 4c), the Cu_xONPs_{60}/GF_{400} electrode displays a couple of sharp redox peaks, indicating an excellent electrocatalytic activity of the Cu_xONPs_{60}/GF_{400} electrode towards H_2O_2 detection. Meanwhile, the Cu_xONPs_{60}/GF_{400} electrode shows an obvious reduction peak at pH = 7.15 (Fig. S6†), which means that the electrode can be applied to a physiological environment. The low detection limit and the linear range of the Cu_xONPs_{60}/GF_{400} electrode for H_2O_2 were measured by differential pulse voltammetry (DPV). As shown in Fig. 5a, the Cu_xONPs_{60}/GF_{400} electrode displays two linear responses for H_2O_2 detection with a good sensitivity of 56.25 μA mM^{-1} cm^{-2} and a low detection limit of 0.023 μM in the range of 0.07–1.13 μM (Fig. 5b), whilst displaying an ultrahigh sensitivity of 3437.5 μA mM^{-1} cm^{-2} in the range of 1.20–133 μM (Fig. 5c). The reason for two linear relationships herein was probably caused by the different H_2O_2 absorption and activation on the Cu_xONPs_{60}/GF_{400} electrode catalyst under different H_2O_2 concentrations.[32] At extremely low H_2O_2 concentration, the electrocatalytic process is dominated by H_2O_2 absorption, but at high H_2O_2 concentration, the process is dominated by H_2O_2 activation. Accordingly, the low detection limit obtained at the Cu_xONPs_{60}/GF_{400} electrode was estimated to be 0.023 μM (S/N = 3). As a contrast, the sensing performances of recently reported H_2O_2 sensors based on copper-based electrodes are shown in Table S2.†[32–41] Detection limit of 0.023 μM and linear range of 0.07–133 μM achieved by using the Cu_xONPs_{60}/GF_{400}. The overall performance of Cu_xONPs_{60}/GF_{400} exceed the most of copper-based electrodes, which benefiting from the unique

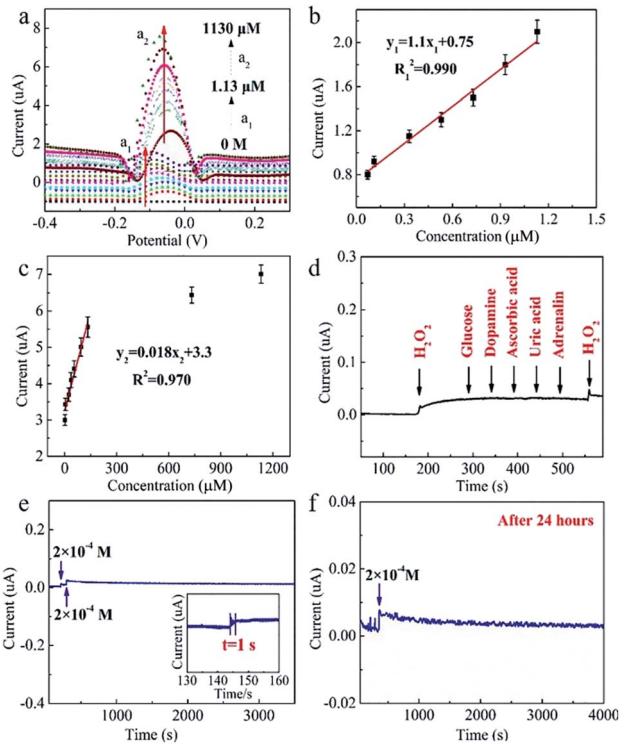

Fig. 5 (a) DPVs of the Cu_xONPs_{60}/GF_{400} electrode in PBS (pH = 7.15) of various H_2O_2 concentrations. The concentration of H_2O_2 is from 0.07 μM to 1.13 mM, scan rate: 50 mV s^{-1}. (b) The fitting curves of reductive current *vs.* concentration of H_2O_2 (0.07, 0.09, 0.11, 0.13, 0.33, 0.53, 0.73, 0.93, 1.13 μM). (c) The fitting curve of current response *vs.* H_2O_2 concentration (1.2, 5.2, 9.2, 13.2, 53.2, 93.2, 133, 733, 1130 μM). (d) Amperometric responses of Cu_xONPs_{60}/GF_{400} electrode at potential of −0.15 V in the 0.1 M PBS with 0.2 mM H_2O_2, 0.04 mM glucose, 0.04 mM dopamine, 0.04 mM ascorbic acid, 0.04 mM uric acid and 0.04 mM adrenalin. (e) Amperometric curve of the Cu_xONPs_{60}/GF_{400} consistently adding 0.2 mM H_2O_2 under gentle agitation. (f) The amperometric curve of the same Cu_xONPs_{60}/GF_{400} after 24 h with addition of 0.2 mM H_2O_2.

This journal is © The Royal Society of Chemistry 2019

Open Access Article. Published on 09 September 2019. Downloaded on 1/22/2026 3:10:54 AM.
This article is licensed under a Creative Commons Attribution-NonCommercial 3.0 Unported Licence.

Table 1 Determination of H_2O_2 in real samples at the Cu_xONPs_{60}/GF_{400} microelectrode ($n = 3$)

Sample	Added (μM)	Founded (μM)	Recovery (%)	Repeatability (% RSD)
Milk	0.47	0.49	104.3	4.01
	0.60	0.58	96.7	3.15
	5.30	5.39	101.7	3.08
	94.10	94.83	100.8	2.15
Human Serum	0.47	0.48	102.1	3.34
	0.60	0.57	95.0	2.08
	5.30	6.11	115.3	4.10
	94.10	95.06	101.0	4.05

microfiber architecture and synergetic effect as well as strong coupling between components with countless active sites and boosted electrons transport. In addition, few group attempt for electrochemical detection of H_2O_2 on fiber electrode.

The selectivity test of the Cu_xONPs_{60}/GF_{400} electrode was carried out in 0.1 M phosphate buffer solution (PBS). 0.2 mM H_2O_2 was added, followed by 0.04 mM glucose, 0.04 mM dopamine, 0.04 mM ascorbic acid, 0.04 mM uric acid and 0.04 mM adrenalin, respectively. As shown in Fig. 5d, after adding 0.2 mM H_2O_2, a distinct current response was observed, and there was almost no change in the peak current in the presence of the interferents. In addition, when a further 0.2 mM H_2O_2 was added, the current signal showed the same response as after the first H_2O_2 addition, indicating the excellent selectivity of the Cu_xONPs_{60}/GF_{400} electrode. The Cu_xONPs_{60}/GF_{400} electrode shows a response time of H_2O_2 detection within 1 s, indicating it tracks very quickly (Fig. 5e inset). The peak current barely changed after 3500 s (Fig. 5e), and after storing at room temperature for 24 h, the response signal of the Cu_xONPs_{60}/GF_{400} electrode remains 98% of its original response for H_2O_2 detection (Fig. 5f), revealing a good operational stability of the Cu_xONPs_{60}/GF_{400} electrode.

Detection of H_2O_2 in milk and human serum

The Cu_xONPs_{60}/GF_{400} electrode was used for the determination of 0.47, 0.60, 5.30, and 94.10 μM H_2O_2 in diluted milk and diluted human serum samples (Table 1 and Fig. S7 and S8†), respectively. The recovery rates calculated according to the calibration curves (Fig. 5b and c) were 104.3%, 96.7%, 101.7% and 100.8% for milk, and 102.1%, 95.0%, 115.3% and 101.0% for human serum, respectively, the relative standard deviation were less than 4.10% for $n = 3$, indicating that the Cu_xONPs_{60}/GF_{400} electrode is effective for H_2O_2 detection in a biological system.

Conclusions

In summary, we have fabricated a graphene fiber electrode modified with well-dispersed and superfine copper oxide nanoparticles derived from electrodeposition self-assembly of a copper-based metal organic frameworks. The as-prepared Cu_xONPs/graphene fiber electrode exhibits a high number of active sites and enhanced electrode exhibits a high number of active sites and enhanced electron-transfer ability. It shows highly efficient electro-catalytic activity for nonenzymatic electrochemical H_2O_2 detection, greater than any previously reported Cu_xONPs-based electrodes. This work provides a simple method for the rapid production of a novel fiber electrode for electrochemical sensor applications.

Conflicts of interest

There are no conflicts to declare.

Acknowledgements

This work was supported by the NSFC (21575014, 21905025), Beijing Natural Science Foundation (2184122), the Fundamental Research Funds for the Central Universities (2018CX01017), Beijing Institute of Technology Research Fund Program for Young Scholars, the project of State Key Laboratory of Explosion Science and Technology (Beijing Institute of Technology, YBKT18-03), and Analysis & Testing Center, Beijing Institute of Technology.

References

1 J. Zhang, J. Han, Z. Shi, Y. Ju, Z. Zhang and M. Gu, *Appl. Surf. Sci.*, 2019, **465**, 357–361.
2 L. Gao, J. Zhuang, L. Nie, J. Zhang, Y. Zhang, N. Gu, T. Wang, J. Feng, D. Yang, S. Perrett and X. Yan, *Nat. Nanotechnol.*, 2007, **2**, 577.
3 Z. Zhang, J. Hao, W. Yang, B. Lu, X. Ke, B. Zhang and J. Tang, *ACS Appl. Mater. Interfaces*, 2013, **5**, 3809–3815.
4 F. Natalio, R. André, A. F. Hartog, B. Stoll, K. P. Jochum, R. Wever and W. Tremel, *Nat. Nanotechnol.*, 2012, **7**, 530.
5 P. Pengo, S. Polizzi, L. Pasquato and P. Scrimin, *J. Am. Chem. Soc.*, 2005, **127**, 1616–1617.
6 W. Shi, X. Zhang, S. He and Y. Huang, *Chem. Commun.*, 2011, **47**, 10785–10787.
7 W. Chen, J. Chen, A. L. Liu, L. M. Wang, G. W. Li and X. H. Lin, *ChemCatChem*, 2011, **3**, 1151–1154.
8 X. X. Wang, Q. Wu, Z. Shan and Q. M. Huang, *Biosens. Bioelectron.*, 2011, **26**, 3614–3619.
9 P. Roy, Z. H. Lin, C. T. Liang and H. T. Chang, *Chem. Commun.*, 2012, **48**, 4079–4081.
10 Z. Chen, J. J. Yin, Y. T. Zhou, Y. Zhang, L. Song, M. Song, S. Hu and N. Gu, *ACS Nano*, 2012, **6**, 4001–4012.
11 M. Baghayeri, H. Alinezhad, M. Tarahomi, M. Fayazi, M. Ghanei-Motlagh and B. Maleki, *Appl. Surf. Sci.*, 2019, **478**, 87–93.
12 J. Cai, S. Ding, G. Chen, Y. Sun and Q. Xie, *Appl. Surf. Sci.*, 2018, **456**, 302–306.
13 K. Zhang, N. Zhang, H. Cai and C. Wang, *Microchim. Acta*, 2012, **176**, 137–142.
14 L. Lu and X. Huang, *Microchim. Acta*, 2011, **175**, 151–157.
15 J. Huang, Y. Zhu, H. Zhong, X. Yang and C. Li, *ACS Appl. Mater. Interfaces*, 2014, **6**, 7055–7062.

Open Access Article. Published on 09 September 2019. Downloaded on 1/22/2026 3:10:54 AM.
This article is licensed under a Creative Commons Attribution-NonCommercial 3.0 Unported Licence.

16 L. Zhou, L. Kuai, W. Li and B. Geng, *ACS Appl. Mater. Interfaces*, 2012, **4**, 6463–6467.
17 R. Agarwal, K. Verma, N. K. Agrawal, R. K. Duchaniya and R. Singh, *Appl. Therm. Eng.*, 2016, **102**, 1024–1036.
18 C. Yang, X. Su, F. Xiao, J. Jian and J. Wang, *Sens. Actuators, B*, 2011, **158**, 299–303.
19 X. Zhang, S. Sun, J. Lv, L. Tang, C. Kong, X. Song and Z. Yang, *J. Mater. Chem. A*, 2014, **2**, 10073–10080.
20 C. Kong, L. Tang, X. Zhang, S. Sun, S. Yang, X. Song and Z. Yang, *J. Mater. Chem. A*, 2014, **2**, 7306–7312.
21 Y. Sun, M. Luo, Y. Qin, S. Zhu, Y. Li, N. Xu, X. Meng, Q. Ren, L. Wang and S. Guo, *ACS Appl. Mater. Interfaces*, 2017, **9**, 34715–34721.
22 Y. Hu, Z. Zhang and C. Yang, *Anal. Chim. Acta*, 2007, **601**, 95.
23 X. Zhu, X. Niu, H. Zhao and M. Lan, *Sens. Actuators, B*, 2014, **195**, 274–280.
24 M. Zhang, Y. Wang, L. Huang, Z. Xu, C. Li and G. Shi, *Adv. Mater.*, 2016, **27**, 6708–6713.
25 V. Gupta, P. Mahbub, P. N. Nesterenko and B. Paull, *Anal. Chim. Acta*, 2018, **1005**, 81–92.
26 A. A. M. Abdurhman, Y. Zhang, G. Zhang and S. Wang, *Anal. Bioanal. Chem.*, 2015, **407**, 8129–8136.
27 M. L. Huffman and B. J. Venton, *Analyst*, 2009, **134**, 18–24.
28 Y. T. Liao, Y. Y. Huang, H. M. Chen, K. Komaguchi, C. H. Hou, J. Henzie, Y. Yamauchi, Y. Ide and K. C. W. Wu, *ACS Appl. Mater. Interfaces*, 2017, **9**, 42425–42429.
29 M. Zhang, Y. Wang, L. Huang, Z. Xu, C. Li and G. Shi, *Adv. Mater.*, 2015, **27**, 6708–6713.
30 T. Baran, S. Wojtyła, C. Lenardi, A. Vertova, P. Ghigna, E. Achilli, M. Fracchia, S. Rondinini and A. Minguzzi, *ACS Appl. Mater. Interfaces*, 2016, **8**, 21250–21260.
31 X. Sun, S. Guo, Y. Liu and S. Sun, *Nano Lett.*, 2012, **12**, 4859–4863.
32 W. Meng, S. Xu, L. Dai, Y. Li, J. Zhu and L. Wang, *Electrochim. Acta*, 2017, **230**, 324–332.
33 F. Xu, M. Deng, G. Li, S. Chen and L. Wang, *Electrochim. Acta*, 2013, **88**, 59–65.
34 H. Song, C. Ma, L. You, Z. Cheng, X. Zhang, B. Yin, Y. Ni and K. Zhang, *Microchim. Acta*, 2015, **182**, 1543–1549.
35 B. B. Jiang, X. W. Wei, F. H. Wu, K. L. Wu, L. Chen, G. Z. Yuan, C. Dong and Y. Ye, *Microchim. Acta*, 2014, **181**, 1463–1470.
36 M. Liu, R. Liu and W. Chen, *Biosens. Bioelectron.*, 2013, **45**, 206–212.
37 C. Zhang, M. Wang, L. Liu, X. Yang and X. Xu, *Electrochem. Commun.*, 2013, **33**, 131–134.
38 S. Li, Y. Zheng, G. W. Qin, Y. Ren, W. Pei and L. Zuo, *Talanta*, 2011, **85**, 1260–1264.
39 Y. K. Hsu, Y. C. Chen and Y. G. Lin, *Appl. Surf. Sci.*, 2015, **354**, 85–89.
40 A. Gu, G. Wang, J. Gu, X. Zhang and B. Fang, *Electrochim. Acta*, 2010, **55**, 7182–7187.
41 J. Huang, Y. Zhu, H. Zhong, X. Yang and C. Li, *ACS Appl. Mater. Interfaces*, 2014, **6**, 7055–7062.

This journal is © The Royal Society of Chemistry 2019